Interligand Electron Transfer Dynamics in $Os^{II}(bpy)_3$: Experimental Results and Model Calculations

J. P. Cushing, C. Butoi, and D. F. Kelley*

Department of Chemistry, Colorado State University, Fort Collins, Colorado 80523-1872

Received: February 17, 1997; In Final Form: June 2, 1997[⊗]

Interligand electron transfer kinetics have been measured in $Os^{II}(bipyridine)_3$ following photoexcitation to the metal-to-ligand charge-transfer state. The measurements are made in room temperature solutions of acetonitrile, ethylene glycol, and glycerol, using time-resolved absorption polarization spectroscopy. The experimental results are strongly dependent on excitation wavelength and are in agreement with the results of reaction/diffusion model calculations. In the calculations, motion along the solvent polarization coordinate is treated as diffusion, and reaction is treated in the nonadiabatic (acetonitrile) or adiabatic (ethylene glycol) limits. The adjustable parameters of the model are the interligand electronic coupling and the solvent polarization barrier height, which are taken to be 15 and 500 cm^{-1}, respectively. The relaxation processes giving rise to the observed kinetic components are discussed.

Introduction

The photophysics of ruthenium(II) and osmium(II) trisdiimines continue to be of great interest. Interest in these compounds, specifically $Ru(bpy)_3^{2+}$, (bpy = 2,2′-bipyridine), originally stems from their potential application in solar energy conversion. These complexes have D_3 symmetry and a d^6 low-spin electron configuration. They have a pseudo-octahedral geometry and thus no net dipole in the ground electronic state. Photoexcitation results in a triplet metal-to-ligand charge-transfer (MLCT) state, which is best described as a 3+ metal ion with an electron in the ligand π^* orbitals. Despite the apparent simplicity of $Ru^{II}(bpy)_3$ and related compounds, their spectroscopy, photophysics, and photochemistry have proven to be rather complicated, resulting in controversial and often conflicting interpretations of experimental results. Two fundamentally important questions have been extensively discussed in the literature. First, is the lowest excited state best described as having the excited electron localized on a single ligand or delocalized over all three ligands? Second, if the electron is localized, what is the time scale for interligand electron transfer (ILET) and what controls the ILET rate? It is important to note that if the electron is delocalized, then the MLCT state has no net dipole, whereas localization implies a large dipole. The presence or absence of a dipole can have profound effects on the excited-state dynamics.

The answers to both of the above questions depend on the magnitude of the coupling between the ligands, H_{ILET}. It is now generally agreed that in the case of $Ru^{II}(bpy)_3$ and $Os^{II}(bpy)_3$ in polar solvents and glasses the electron is localized on a single ligand.[1−20] The same may be true for the similar compound $Ru^{II}(phenanthroline)_3$, although this point remains controversial.[12,21,22] Localization establishes a limit on the size of the coupling, H_{ILET}, by the following consideration. As mentioned above, the localized excited state has a large dipole associated with it. In a fluctuating polar solvent, the energy of the dipole varies by an amount comparable to kT. It is important to note that the three metal−ligand moieties have energies which can vary independently. As a result, delocalization of the electron in the π^* orbitals requires a coupling which is large compared to kT. We therefore conclude that in all cases, H_{ILET} must be less than a few hundred wavenumbers.

Estimates of ILET times in low-temperature crystals have been made from line width measurements. It has recently been shown that,[11] in the case of $Ru^{II}(bpy)_3$, the electron is localized on a single ligand in 1.8 K and that line widths indicate the coupling is <0.1 cm^{-1}. A corresponding long interligand electron-transfer time of ∼10 ns is estimated. In contrast, spectroscopic results on $Os^{II}(bpy)_3$ in low-temperature $Zn(PF_6)_2$ crystals indicate that the MLCT state is delocalized.[12,16] In this case, H_{ILET} is estimated to be about 2 cm^{-1}. The extent of the coupling is environment dependent, and larger couplings are observed in other crystal environments.[12] It should be emphasized that low-temperature crystal results yield H_{ILET} values for only the lowest vibronic level. Different values may be obtained at room temperature, when various vibrational modes are excited.

Several methods have been used in attempts to measure ILET rates in solutions and glasses. Excited-state resonance Raman studies have been interpreted in terms of relatively rapid ILET, less than a few nanoseconds.[1−3] However, other Raman measurements were interpreted in terms of slow ILET.[23] The interpretation of fast ILET is consistent with the results of intramolecular quenching in $Ru^{II}(bpy)_3$(electron acceptor) systems, which indicated ILET occurs in less than a few hundred picoseconds.[24] Direct measurement of ILET rates in solutions and glasses has been somewhat problematic. The most obvious approach is to photoexcite the molecule with polarized light and measure the time-dependent emission polarization. The idea of these experiments is that a particular metal−ligand moiety will be photoselected upon excitation, and the emission will depolarize as ILET occurs. However, this approach is complicated by equilibration of the different triplet levels, and since the different triplet levels mix with singlets having different polarizations, this type of experiment largely measures the rate of spin/lattice relaxation.[9] The ILET times in $Ru^{II}(bpy)_3$ and $Os^{II}(bpy)_3$ in room temperature polar solvents have been measured directly by time-resolved absorption polarization spectroscopy. In both cases, the ILET times were tens to hundreds of picoseconds, and were dependent upon the solvent relaxation time.[18−20]

* To whom correspondence should be addressed.

[⊗] Abstract published in *Advance ACS Abstracts,* September 1, 1997.

S1089-5639(97)00587-2 CCC: $14.00

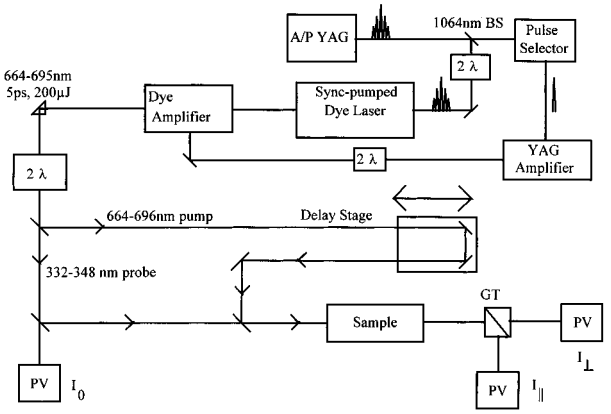

Figure 1. Experimental apparatus used to measure time-resolved absorption polarization data. The following abbreviations were used: A/P YAG, active/passive mode-locked YAG oscillator; GT, Glan-Taylor polarizer; PV, photovoltaic.

In the present paper, we present a detailed study of the ILET dynamics in $Os^{II}(bpy)_3$ in room temperature polar solvents using time-resolved absorption polarization spectroscopy. These experiments are based on the premise that the MLCT state is inherently ligand localized, and the metal−bipyridine oscillators may therefore be treated independently. The basic idea of these experiments is the following. Photoexcitation with polarized light accomplishes two types of photoselection. In this case, polarized light photoselects a certain population of the molecules, and introduces an anisotropy in that population. Specifically, polarized light photoselects those $Os^{II}(bpy)_3$ ions with an Os−bpy moiety most closely aligned with the electric field of the excitation light. This corresponds to the electric vector of the light being in the plane which is perpendicular to the D_3 axis of the ion. In addition to the above photoselection, excitation also photoselects the particular Os−bpy moiety most closely aligned with the electric field of the light. It is important to note that this latter type of photoselection is lost as ILET occurs. The system is subsequently probed by measuring the time-dependent polarization of the $bpy^{\bullet-}$ absorption. These data give the time dependence of ILET through a very straightforward analysis. The reason for studying $Os^{II}(bpy)_3$ (as opposed to $Ru^{II}(bpy)_3$) is a simple technical one. It is much easier using picosecond YAG/dye lasers to generate tunable light near the ∼690 nm $Os^{II}(bpy)_3$ absorption onset than near the ∼480 nm $Ru^{II}(bpy)_3$ absorption onset. In the present results, we have determined the ILET dynamics as functions of excitation wavelength and the rates of solvent relaxation. In particular we have examined the dynamics in solvents which relax very rapidly (acetonitrile), relax slowly (ethylene glycol), and are glasslike (glycerol). The experimental results are compared to the results of model calculations involving reaction (ILET) and diffusion on potential surfaces which correspond to the electron being localized on the different bipyridines. A preliminary account of this work (lacking all of the calculational results) has recently been published.[20]

Experimental Methods

The experimental apparatus used in these studies is based on an active/passive mode-locked Nd:YAG laser which sync-pumps and amplifies a dye laser (see Figure 1). The samples were excited with ∼10 ps (full width at half-maximum) pulses that range in wavelength from 664 to 695 nm. Wavelengths blue of 670 nm were generated using DCM dye dissolved in a 2:3 mixture of propylene carbonate and ethylene glycol in the dye oscillator and dye amplifier chain. Wavelengths red of 670 nm were generated using LDS-698 dissolved in methanol in the dye oscillator and DCM dye dissolved in a 2:3 mixture of propylene carbonate and ethylene glycol in the amplifier chain. At the sample, the pump light was horizontally polarized, had an energy less than 50 μJ, and was focused to a spot size of ∼0.5 mm. The probe light for all but the 355 nm probe experiments was generated by frequency doubling the dye fundamental laser light. These probe wavelengths also have a fwhm pulse width of around 10 ps. The 355 probe was generated by mixing 1064 and 532 nm light. The 355 nm light has the same fwhm pulse width as the YAG fundamental, ∼30 ps. In all cases, the probe light was spacially filtered and then passed through a $\lambda/4$ waveplate with the azimuthal angle chosen such that equal components of light polarized parallel and perpendicular with respect to the pump light were produced. The probe beam was then focused onto the sample with a spot size somewhat smaller than that of the pump beam. After passing through the sample, the pump light was removed and the probe light was passed through a Glan-Taylor polarizer to separate out the parallel and perpendicular polarized components. Reference, parallel, and perpendicular probe intensities were detected using EG&G UV-100-BQ photovoltaics. A U340 filter was placed in front of each detector to eliminate stray light.

The $Os^{II}(bpy)_3$ $(PF_6)_2$ was a gift from Professor C. M. Elliott and was used without further purification. All the solvents were spectral grade and used without further purification. All samples were degassed prior to use to prevent photoreaction with oxygen. The acetonitrile samples were placed in 2 mm path length quartz cells and were degassed using several cycles of freeze−pump−thaw. The ethylene glycol samples were also placed in 2 mm path length quartz cells. These samples were degassed by attaching the cell to a vacuum line for approximately 20 min in the dark. The glycerol samples were in 1 cm path length quartz cells and were degassed by attaching the cell to the vacuum line for several hours in the dark. The cell was then allowed to equilibrate (degas) overnight (in the dark), and the vacuum procedure was repeated the following day. All experiments were performed with the samples at room temperature.

Experimental Results

$Os^{II}(bpy)_3$ is a low spin, d^6 pseudo-octahedral complex with D_3 symmetry and no permanent dipole in its ground electronic state. The lowest excited state is triplet MLCT and is produced when one of the 5d electrons on the osmium is excited to a π^* orbital on a single bipyridine ligand. Thus, the MLCT excited state is best described as $Os^{III}(bpy)_2(bpy^{\bullet-})$. MLCT absorption occurs in the 640−720 nm region for $Os^{II}(bpy)_3$ (pump light), while bipyridical radical anion absorption is in the 320−390 nm region[25,26] (probe light). The MLCT absorption is polarized along the metal-to-ligand axis, and the bipyridine radical anion $\pi-\pi^*$ absorption is polarized along the long axis of the bipyridine,[26] at 90° with respect to the initial absorption oscillator. Following MLCT excitation, the excited electron can either stay on the nascent bipyridine or hop to an adjacent ligand. Different polarization components of the probe light will be preferentially absorbed depending on the location of excited electron. This can be measured in terms of the time-dependent depolarization ratio $r(t)$, given by the expression

$$r(t) = \frac{A_{||} - A_{\perp}}{A_{||} + 2A_{\perp}} \tag{1}$$

where $A_{||}$ is absorbance of the probe light that has the same polarization as the pump light and $A_{\perp}$ is absorbance of the probe

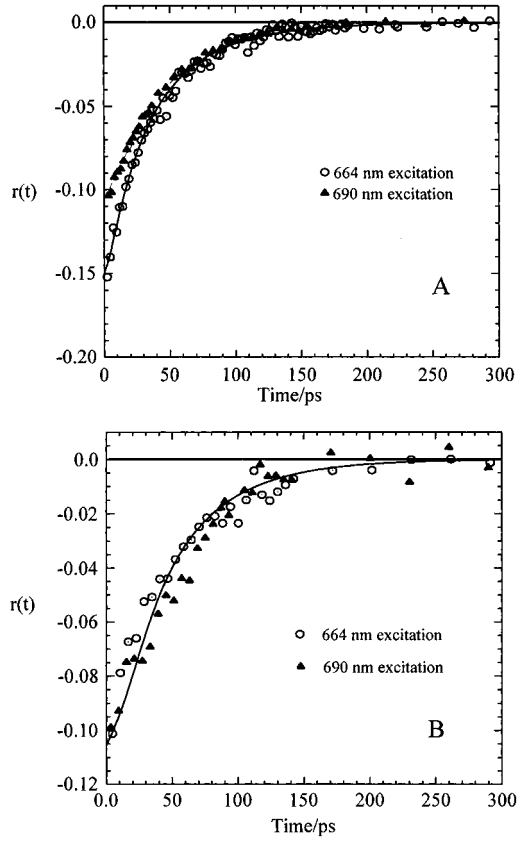

Figure 2. Experimental plots of the depolarization ratio for $Os^{II}(bpy)_3$ in room temperature acetonitrile. (A) Two pump and probe wavelengths, 664 nm pump/332 nm probe and 690 nm pump/345 nm probe, are shown here by the circles and triangles, respectively. The solid curve and dotted-dashed curve are biexponential fits to the 664 nm and 690 nm data, respectively. Both fits have $k_{ET} = (130\ ps)^{-1}$, $6D_S = (51\ ps)^{-1}$, and $C_2 = -0.08$. The 664 nm fit has $C_1 = -0.08$, and the 690 nm fit has $C_1 = -0.04$. (B) Two pump wavelengths, 664 nm and 690 nm, are shown here by the circles and triangles, respectively. 355 nm light was used as the probe for both pump wavelengths. The solid line is a biexponential fit with $C_1 = -0.05$, $C_2 = -0.085$, $k_{ET} = (130\ ps)^{-1}$, and $6D_S = (51\ ps)^{-1}$.

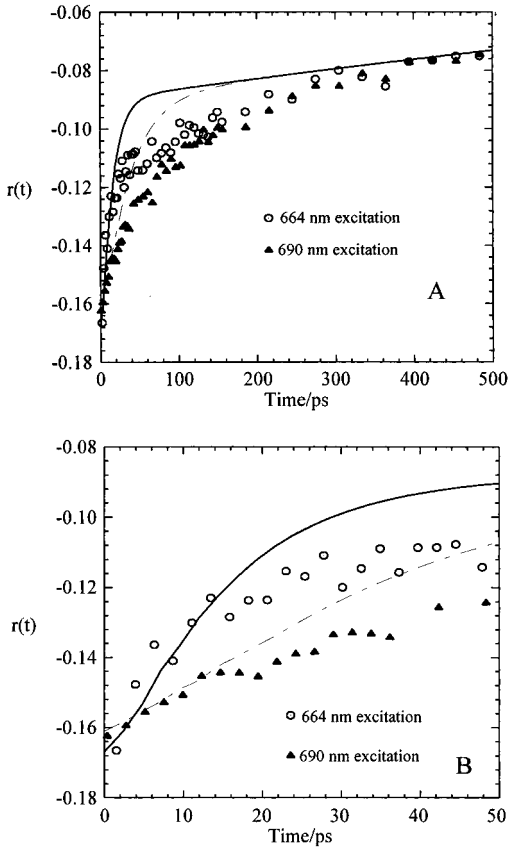

Figure 3. Experimental plots of the depolarization ratio for $Os^{II}(bpy)_3$ in room temperature ethylene glycol. (A) Two pump and probe wavelengths, 664 nm pump/332 nm probe and 690 nm pump/345 nm probe, are shown here by the circles and triangles, respectively. The solid curve and dotted-dashed curve are biexponential fits to the 664 nm and 690 nm data, respectively. The 664 nm pump fit has $C_1 = C_2 = -0.09$, $k_{ET} = (40\ ps)^{-1}$, and $6D_S = (2400\ ps)^{-1}$. The 690 nm pump fit has $C_1 = -0.08$, $C_2 = -0.09$, $k_{ET} = (100\ ps)^{-1}$, and $6D_S = (2400\ ps)^{-1}$. (B) This is an enlarged section of the first 50 ps of plot A.

light that has an orthogonal polarization to that of the pump light. At $t = 0$, just after MLCT excitation, the probe absorbance should be mostly orthogonal to that of the pump and therefore $r(0)$ should be negative. As the electron hops or as the molecule rotates, this ratio will become less negative. It is important to note that several transitions of different polarizations may contribute to the MLCT absorption. As a result, the MLCT and probe polarizations may not be completely orthogonal. This will decrease the magnitude of the depolarization signal, but will not affect the kinetics. For an ILET reaction characterized by a single rate constant, the depolarization ratio for the situation described above should fit to a biexponential[27−29] (see eq 20)

$$r(t) = C_1 \exp[-(6D_s + 3k_{ET})t] + C_2 \exp(-6D_s t) \quad (2)$$

where k_{ET} is the ILET rate constant and D_s is the rotational diffusion constant for a spherical rotor (we have approximated the complex as a spherical molecule). If there are no transitions other than the MLCT and bipyridical radical anion absorptions, these transitions have polarizations which are completely orthogonal, and the absorptions do not overlap, then we obtain $C_1 = C_2 = -0.1$. If the above conditions are not completely met, then C_1 and C_2 will have values less negative than -0.1.

Time-dependent depolarization results for $Os^{II}(bpy)_3$ in acetonitrile, ethylene glycol, and glycerol are shown in Figures 2−4. The depolarization curves, $r(t)$, are calculated from time-dependent pump−probe absorption data using eq 1. Two pump wavelengths, 664 and 690 nm, are used for photoexcitation. The corresponding probe wavelengths are frequency-doubled pump, 332 and 345 nm, respectively. Shown with the experimental curves are calculated biexponential depolarization curves (see eq 2). Comparison with the experimental results requires that the calculated curve be convoluted with the known instrument response function. This convolution is accomplished in the following way. From calculated values of $r(t)$ and total (experimental) transient absorbances ($A_{||} + 2A_{\perp}$), time-dependent $A_{||}$ and $A_{\perp}$ curves are calculated and then convoluted with the instrument response function. The resulting curves are used to calculate a convoluted $r(t)$ curve. (It is incorrect to simply convolute $r(t)$ with the instrument response function. The spectrometer experimentally generates convoluted absorbance curves, from which $r(t)$ is obtained.) This biexponential form for the time-dependent depolarization of $Os^{II}(bpy)_3$ should fit the data if the reaction is characterized by a unique, time-independent electron-transfer rate constant.

The depolarization curves for $Os^{II}(bpy)_3$ in acetonitrile are shown in Figure 2. The depolarization curve corresponding to $Os^{II}(bpy)_3$ excited at 664 nm fits well to a biexponential with 23 and 51 ps components and both C_1 and C_2 coefficients being -0.08. This corresponds to an ILET rate of $(130\ ps)^{-1}$ and a rotational diffusion rate of $(51\ ps)^{-1}$. The rotational diffusion rate of $(51\ ps)^{-1}$ is consistent with the rate obtained from the

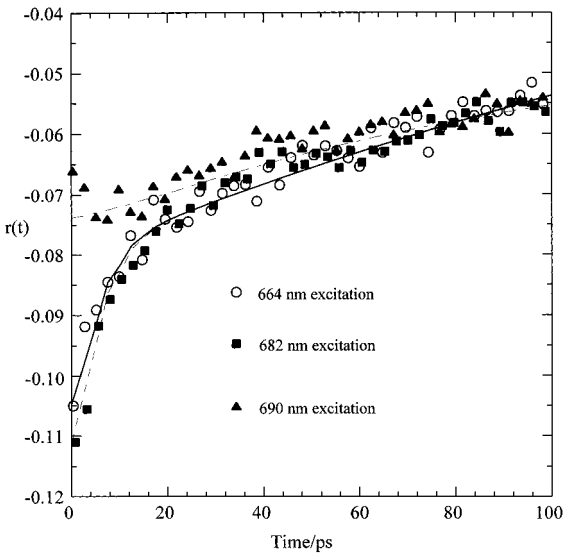

Figure 4. Experimental plots of the depolarization ratio for $Os^{II}(bpy)_3$ in room temperature glycerol. Three pump and probe wavelengths, 664 nm pump/332 nm probe, 682 nm pump/341 nm probe, and 690 nm pump/345 nm probe, are shown here by the open circles, squares, and triangles, respectively. The solid and dashed curves are biexponential fits to the 664 nm and 682 nm data, respectively. The 664 nm pump fit has $C_1 = -0.04$, $C_2 = -0.08$, and $k_{ET} = (10\ ps)^{-1}$. The 682 nm pump fit has $C_1 = -0.06$, $C_2 = -0.08$, and $k_{ET} = (10\ ps)^{-1}$. In both cases the slow component is fit to a 250 ps decay.

Stokes−Einstein theory of rotational diffusion, and a hydrodynamic radius of 5.2 Å, which is reasonable for this molecule.[29] The depolarization of $Os^{II}(bpy)_3$ excited at 690 nm also fits to a biexponential with the same time constants. The fit differs from that obtained with 664 nm excitation in that $C_1 = -0.04$ instead of -0.08. The differences in C_1 values between the 664 and 690 nm depolarizations are due to differences in the probe wavelengths. This is confirmed when the same probe wavelength is used for both excitation wavelengths. Figure 2B shows results from experiments in which 355 nm light was used as the probe wavelength (35 ps temporal resolution as opposed to 10 ps resolution for the doubled pump) for both 664 and 690 nm excitation. The resulting depolarization curves are indistinguishable and fit to a biexponential with 23 and 51 ps components with $C_1 = -0.05$ and $C_2 = -0.085$. This result also shows that that the same electronic state is excited by 664 and 690 nm light.

The depolarization curves for $Os^{II}(bpy)_3$ in ethylene glycol are shown in Figure 3. Figure 3 shows the 664 and 690 nm data with biexponential fits that match short and long time components of the data. As seen in the figure, neither the 664 nm nor the 690 nm data fit to a biexponential. Furthermore, unlike the behavior observed in acetonitrile, there is an excitation wavelength dependence to the depolarization. Figure 3B shows this behavior at short times. The 664 nm excitation depolarization curve has a much faster short time component than the 690 nm excitation depolarization.

The depolarization curves for $Os^{II}(bpy)_3$ in glycerol are shown in Figure 4. For this solvent, three excitation wavelengths were used, 664, 682, and 690 nm. As is seen in the figure, there is a short time fast component (fit to 10 ps) in the 664 nm excitation data, which is slightly larger in the 682 nm excitation depolarization and is absent in the 690 nm excitation data. In the 682 and 664 nm cases, the slow depolarization component is $(250\ ps)^{-1}$. This value does not correspond to the rotational diffusion rate of $Os^{II}(bpy)_3$ in glycerol but was chosen to fit the data. A somewhat slower decay fits the 690 nm excitation data.

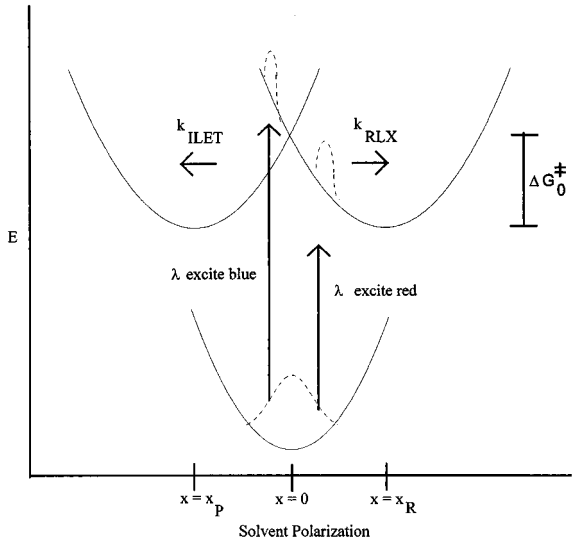

Figure 5. Schematic diagram of the free energy surfaces corresponding to the ground and nonadiabatic excited states of $Os^{II}(bpy)_3$. The solvent polarization coordinate is represented by the ordinate. The arrows represent 690 (red) and 664 (blue) nm MLCT excitations. The dotted curves represent the ground-state and nascent population distributions. k_{ILET} and k_{RLX} refer to the rate of electron transfer to the product surface and solvent relaxation rates, respectively. x_R and x_P refer to the equilibrium polarizations of the reactant and product states, respectively.

As is seen in the above results, the time-dependent depolarizations are very different for fast and slowly relaxing solvents. This indicates that the ILET kinetics are very different for the three solvents. In the next section, we present a semiquantitative model to explain these results.

Model for ILET in $Os^{II}(bpy)_3$

The central consideration in understanding the ILET dynamics is that the ground state of $Os^{II}(bpy)_3$ has no permanent dipole moment, whereas the excited state has a relatively large dipole. It is the interaction of this dipole with the surrounding polar solvent which gives rise to the solvent dependence of the ILET kinetics, and hence the depolarization kinetics.

The depolarization kinetics presented above may be understood in terms of a reaction/diffusion model. This model requires calculation of the dynamics occurring on the potential surfaces corresponding to different ligand-localized states, as depicted in Figures 5 and 6. The basic idea of this model is as follows. Potential energy surfaces (energy versus solvent polarization), corresponding to the electron being localized on different bipyridines, are constructed. Because the reactant and product states have different equilibrium solvent polarizations, there is an outer sphere barrier to ILET. Polarized photoexcitation projects some of the ground state population onto the reactant excited-state surface. The exact location of the nascent excited-state population on this surface is excitation wavelength dependent, but in all cases is fairly close to the ILET transition state. The population evolves in time according to the reaction/diffusion equations. At any given time the total amount of population on the initial (reactant) and the other (product) surfaces may be calculated. Using these populations and photoselection theory, time-dependent depolarization ratios may be calculated and compared with experimental results. The above calculations may be divided into several parts. The first part is the construction of the potential energy surfaces and the calculation of the transition (ILET) rates between them. This involves the use of several parameters, which will be adjusted to fit the experimental results. Second is the determination of

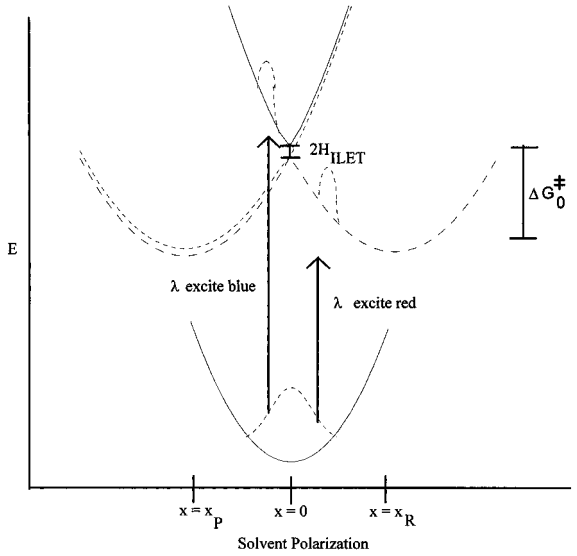

Figure 6. Schematic diagram of the free energy surfaces corresponding to the ground and adiabatic excited states of $Os^{II}(bpy)_3$. The solvent polarization coordinate is represented by the ordinate. The arrows represent 690 (red) and 664 (blue) nm MLCT excitations. The dotted curves represent the ground state and nascent reactant population. Determination of reactant and product populations is dependent on the coefficients which relate the nonadiabatic and adiabatic potential energy surfaces. x_R and x_P refer to the equilibrium polarizations of the reactant and product states, respectively.

the wavelength-dependent, nascent ($t = 0$) population distribution on the reactant surface. Third is the numerical simulation of the reaction/diffusion process to obtain time-dependent reactant and product populations. Finally, photoselection theory is applied to calculate time-dependent depolarization ratios. The details and approximations involved in each part of the calculations are discussed below.

The specifics of how the potential surfaces are calculated and how the reaction/diffusion calculation is performed depend upon if the ILET reaction is in the adiabatic or nonadiabatic limit. In the nonadiabatic case, the probability of reactant to product surface crossing is low, while the opposite is true in the adiabatic case. These two cases are defined by the adiabaticity parameter,[30] H_A. The adiabaticity factor is derived from Landau−Zener theory[30,31] and for this system is given by

$$H_A = \frac{\pi H^2_{ILET}\tau}{\hbar\lambda} \tag{3}$$

where τ is the average solvent relaxation time,[32] H_{ILET} is the magnitude of the coupling between the reactant and product states, and, in this case, $\lambda = \Delta G^{\ddagger}$. The reaction is nonadiabatic when $H_A \ll 1$ and adiabatic when $H_A \gg 1$. It is important to note that with a constant value of H_{ILET}, the reaction can be nonadiabatic in one solvent and adiabatic in another solvent. If the two solvents result in the same coupling between the ligands and have similar dielectric properties, i.e., produce the same solvent-induced barrier height, then different solvent relaxation times will result in different adiabaticity factors. Acetonitrile and ethylene glycol have fairly similar dielectric properties, while acetonitrile relaxes very rapidly and ethylene glycol very slowly. We therefore anticipate that the dynamics in acetonitrile and ethylene glycol will fall into the nonadiabatic and adiabatic limits, respectively. We will fit the experimental data assuming that this is the case, using the same values of H_{ILET} and $\Delta G^{\ddagger}$ for both solvents. The values of H_{ILET} and $\Delta G^{\ddagger}$ obtained by fitting the depolarization curves, along with the respective relaxation times, are then shown to be consistent with this expectation.

A two-dimensional approximation has been made in constructing the ground-state, reactant, and product potential surfaces, as shown in Figures 5 and 6. In this approximation we ignore the fact that the excited-state dipoles associated with localization on two different bipyridines are not collinear. ILET rotates the excited-state dipole by 120°. The ILET transition state is where the reactant and product have the same energy. This corresponds to one-half of a charge on both the reactant and product bipyridines. The resulting dipole bisects the 120° angle and has a magnitude one-half that of the reactant or product. Since the energy of a dipole is proportional to the square of its magnitude, the solvation energy of the transition state is one-fourth that of the reactant or product. In the two-dimensional approximation, this transition-state dipole is ignored. As a result, intersection of the excited-state reactant surfaces is taken to occur directly above the center of the spherically symmetric (no dipole) ground state. It follows that in this model, photoexcitation from the bottom of the ground-state well results in population at the transition state. The adjustable parameters in this model are the solvent-induced barrier to ILET, $\Delta G^{\ddagger}$, the energy separation of ground and excited states, and the coupling between adjacent bipyridine ligands, H_{ILET}. The two-dimensional approximation greatly simplifies the model calculations. However, it is a fairly crude approximation of the actual situation. Ignoring the transition-state dipole makes errors in both the position of the transition state and the size of the ILET barrier. Therefore, the results of the model calculations presented below must be viewed as only semiquantitative. Despite this shortcoming, this model will allow the identification and assignment of the observed kinetic components.

The zeroth-order potential energy surfaces are shown in Figure 5 and are defined as follows. The ground state is modeled as a two-dimensional parabolic surface with no permanent dipole and its energy is given by the expression

$$V_G = \lambda x^2 \tag{4}$$

where x is the solvent coordinate and $\lambda = (\Delta G^{\ddagger})$ is the solvent reorganization energy. The excited-state surfaces have energies given by the expressions

$$V_R = \lambda(x-1)^2 + E_0 \tag{5}$$

and

$$V_P = \lambda(x+1)^2 + E_0 \tag{6}$$

where E_0 is the energy difference between the bottom of the ground-state well to the bottom of either excited-state well. The energy of $E_0 + \lambda$ is needed for excitation to the transition state. This transition-state wavelength is taken to be the inflection point of the MLCT absorption onset for $Os^{II}(bpy)_3$, corresponding to about 680 nm. λ is defined as the amount of solvation energy that the reactant in equilibrium with the polar solvent would have if it suddenly lost its dipole. As a result, for this system, λ has the same magnitude as $\Delta G^{\ddagger}$. In principle, values of λ may be calculated from continuum theory using the expression[33]

$$\lambda = \frac{\mu^2}{\alpha^3}\left[\left(\frac{\epsilon_0 - 1}{2\epsilon_0 + 1}\right) - \left(\frac{\epsilon_\infty - 1}{2\epsilon_\infty + 1}\right)\right] \tag{7}$$

where μ is the dipole moment, α is the radius of the dielectric

cavity and ϵ_0 and ϵ_∞ are the low- and high-frequency dielectric constants, respectively. Literature values of the MLCT dipole moment in $Os^{II}(bpy)_3$ are somewhat inconsistent, making evaluation of eq 7 problematic. Solvent-dependent room-temperature absorption spectra[5] indicate that the singlet state has a dipole moment of 13.3 ± 6.6 D. Low-temperature Stark measurements[12] indicate a triplet-state dipole moment of 3 D. To the extent that both states correspond to an electron localized on a single bipyridine ligand, similar values would be expected. As a result of the above uncertainty, the value of λ must be taken as an adjustable parameter. If H_A is small, the probability of reactant−product transitions is small, and we may consider the zeroth-order surfaces to be negligibly perturbed. This is the case in the nonadiabatic ($H_A \ll 1$) limit depicted in Figure 5.

Construction of the potential surfaces is somewhat more complicated in the adiabatic case. In the adiabatic ($H_A \gg 1$) limit, even though H_{ILET} has the same value as before, interaction between the reactant and product surfaces cannot be ignored. In the two-surface case, this leads to a simple avoided crossing of zeroth-order reactant and product curves. The resulting upper and lower curves are separated by $2H_{ILET}$ at $x = 0$. The case of three interacting zeroth-order surfaces is slightly more complicated, as depicted in Figure 6. As in the two-surface case, the adiabatic excited-state surfaces are calculated by applying degenerate perturbation theory[35] to the reactant (R) and two product (P_1,P_2) surfaces described in eqs 5 and 6. Three unperturbed surfaces interact to produce three perturbed surfaces, an upper (U), a lower (L), and an intermediate surface, which resembles the initial product surfaces (P), see Figure 6.

The qualitative dynamics depend on whether the system falls into the adiabatic or nonadiabatic limit. If the solvent relaxes quickly and H_A is much less than 1, then the nascent distribution rapidly relaxes to the bottom of the reactant well, regardless of the excitation wavelength. The reaction can be described by a coupled reaction/diffusion equation, where diffusion maintains Boltzmann distributions in each well and the reaction rate has a direct relationship with the square of the coupling between the ligands. This results in a transition-state theory (TST) expression for the reaction rate constant. If, on the other hand, the solvent relaxes slowly and H_A is greater than 1, then the initial excited-state distribution and hence the excitation wavelength become important in determining the subsequent dynamics. Following excitation below the transition state, the nascent distribution relaxes into the bottom of the reactant well and, like in the fast relaxing solvent, ILET occurs via thermal fluctuations which result in barrier crossing. However, following excitation above the transition state, the dynamics become dependent on the probability of traversing the splitting, $2H_{ILET}$: the greater the splitting, the less probable the transition. In the slow diffusion, adiabatic case Boltzmann distributions are not maintained in either the reactant or the product wells. The dynamics may be described by a coupled reaction/diffusion equation.

The nonadiabatic reaction for acetonitrile solvent is modeled as follows. The time-dependent reactant, $R(t)$, and product, $P(t)$, populations are given by

$$R(t) = \int_{-\infty}^{\infty} r(x,t)\,dx \quad \text{and} \quad P(t) = \int_{-\infty}^{\infty} p(x,t)\,dx \qquad (8)$$

where $r(x,t)$ and $p(x,t)$ are weighted Boltzmann distributions centered about the bottom of the reactant and product wells, respectively

$$r(x,t) \propto \exp\left(-\frac{\lambda(x-1)^2}{kT}\right) \quad \text{and}$$

$$p(x,t) \propto \exp\left(-\frac{\lambda(x+1)^2}{kT}\right) \qquad (9)$$

and $R(t) + P(t) = 1$. In the simplest case, all reaction occurs where the reactant and product curves cross at $x = 0$. Since there are two ligands to which the electron can transfer, the reaction is described at the transition state ($x = 0$) as

$$r(0,t) \underset{k_{NA}}{\overset{2k_{NA}}{\rightleftharpoons}} p(0,t) \qquad (10)$$

where k_{NA} is the A factor for a nonadiabatic reaction,[34] and is given by

$$k_{NA} = \frac{H^2_{ILET}}{2\hbar}\left(\frac{\pi}{\lambda kT}\right)^{1/2} \qquad (11)$$

However, low-frequency modes which couple to ILET permit electron transfer to occur at x values other than 0. In general, we have

$$r(x,t) \underset{k_2(x)}{\overset{2k_1(x)}{\rightleftharpoons}} p(x,t) \qquad (12)$$

If we make the simplest approximation, and ignore the energy dependence of the Franck−Condon factors, then for $x > 0$

$$k_1(x) = k_{NA}\exp\left(\frac{-|\Delta E(x)|}{kT}\right) \quad \text{and} \quad k_2(x) = k_{NA}$$

where ΔE is the energy difference between the reactant and product surfaces at that x value. For values of $x < 0$

$$k_1(x) = k_{NA} \quad \text{and} \quad k_2(x) = k_{NA}\exp\left(\frac{-|\Delta E(x)|}{kT}\right)$$

As stated above, a Boltzmann distribution is maintained in both reactant and product wells. As such, the dynamics are excitation wavelength independent and a transition-state theory electron-transfer rate is obtained. The adjustable parameters in this model are the values of λ and H_{ILET}. Specification of these two parameters determines the potential surfaces and k_{NA}.

In the adiabatic case, the finite rate of diffusion on the surfaces depicted in Figure 6 must be considered. In addition, population can move between these surfaces (ILET).

$$U(x,t) \underset{k_2(x)}{\overset{k_1(x)}{\rightleftharpoons}} L(x,t)\; U(x,t) \underset{k_3(x)}{\overset{k_1(x)}{\rightleftharpoons}} P(x,t)\; P(x,t) \underset{k_4(x)}{\overset{k_1(x)}{\rightleftharpoons}} L(x,t)$$

The rate constants are all based on the rate from upper surface to the lower and product surfaces. In analogy with the nonadiabatic case, we have made the approximation that these rates are the same and independent of x. This rate is designated as k_1 and is related to the probability of the population staying on the upper surface. The probability, $P(x)$, of the population staying on the upper well may be calculated using Landau−Zener theory.[31] The rate is

$$k_1 = \frac{1}{\tau}\exp\left(-\frac{\pi H^2_{ILET}\tau}{2\lambda\hbar}\right) = \frac{1}{\tau}e^{-H_A/2} \qquad (13)$$

As in the nonadiabatic case, x-dependent values of k_2, k_3, and k_4 are obtained by detailed balance from k_1.

Diffusion is modeled using a Smoluchowski equation. For diffusion in one dimension, the change in population with respect to time at a particular x value is given by the expression[36,37]

$$\frac{\partial C(x,t)}{\partial t} = D(t)\left(\frac{\partial^2}{\partial x^2} + \beta\left(\frac{\partial V(x)}{\partial x}\right)\frac{\partial}{\partial x}\right)C(x,t) \qquad (14)$$

where $C(x,t)$ is the population, $V(x)$ refers to the potential surface, $\beta = (1/kT)$, and $D(t)$ is the diffusion constant calculated using[38]

$$\beta D(t) = -\frac{1}{2\lambda}\left(\frac{\mathrm{d}}{\mathrm{d}t}\ln \Delta(t)\right) \qquad (15)$$

Assuming linear response, $\Delta(t) = S(t)$ for the solvent, where $S(t)$ is the frequency response function of a time-dependent Stokes frequency shift experiment.[32] If $S(t)$ is taken to relax exponentially with a time constant τ, then the above equation yields a time-independent diffusion constant:

$$D = \frac{1}{2\beta\lambda\tau} \qquad (16)$$

We have made this approximation, and taken τ to be the average relaxation time observed in the time-dependent Stokes shift experiments.[32] The above reaction/diffusion equations may be integrated numerically. Once the time-dependent populations on the three surfaces have been calculated, they are converted to reactant and product populations. Specifically, populations on the upper, lower, and intermediate surfaces are converted to equivalent populations on the zeroth-order reactant and product surfaces.

The time-dependent reactant and product populations produced by either the adiabatic or nonadiabatic simulations have to be converted to depolarizations in order to compare the results with experiment. This is done using the results of the analysis of the depolarization of a general rotor. It is shown that[39]

$$r(t) = {}^2/_5 P_2(\cos\theta)\exp(-6D_s t) \qquad (17)$$

where $P_2(\cos\theta)$ is the second-order Legendre polynomial, θ is the angle between the pump absorption and probe absorption, $6D_s$ is the inverse of the rotational correlation time and $r(t)$ is the time-dependent depolarization (not to be confused with $r(x,t)$, the time-dependent population on the reactant surface). The probe absorption of interest here is the bipyridical radical anion absorption. Since the electron can hop from one ligand to an adjacent ligand, the polarization of the probe absorption will change with time. This change can be predicted using eq 17, applied to the different pump−probe absorption angles that will occur before and after ILET. In the idealized case, the MLCT excitation is polarized along the metal−ligand axis and the bipyridical radical anion absorption is polarized along the long axis of the bipyridine. That portion of the population that remains on the initially excited ligand, the reactant population, has a 90° angle between the pump and probe absorptions. Therefore, the absorption depolarization due to the reactant becomes

$$r_R(t) = {}^2/_5(-{}^1/_2)\exp(-6D_s t)\,R(t) \qquad (18)$$

That portion of the population that hops to an adjacent ligand, the product population, has a 60° angle between the pump and probe absorptions. Therefore, the absorption depolarization due to the product becomes

$$r_P(t) = {}^2/_5(-{}^1/_8)\exp(-6D_s t)\,P(t) \qquad (19)$$

Summing these two results in the experimentally observed depolarization

$$r(t) = {}^2/_5(A_1 R(t) + A_2 P(t))\exp(-6D_s t) \qquad (20)$$

with $A_1 = -1/2$, and $A_2 = -1/8$. The same result is obtained by photoselection theory.[28] This analysis assumes that all transitions are completely polarized, there is no overlap between these transitions, and there are no other transitions present. If these assumptions are not correct, then the A_1 and A_2 coefficients can be smaller in magnitude. If the electron-transfer reaction is characterized by a single rate constant, k_{ET}, then we have

$$R(t) = {}^1/_3(1 + 2\exp(-3k_{ET}t)) \quad \text{and}$$

$$P(t) = {}^2/_3(1 - \exp(-3k_{ET}t))$$

Inserting these functions into eq 20, eq 2 is recovered, with $C_1 = C_2 = -1/10$. In the more general case, time-dependent absorption depolarizations may be obtained from calculated values of $R(t)$ and $P(t)$.

The results of these calculations are presented in Figures 7 and 8. In all cases a $\Delta G^{\ddagger}$ ($= \lambda$) value of 500 cm^{-1} and an H_{ILET} value of 15 cm^{-1} is assumed. Furthermore, the same values of A_1 and A_2 are used in both solvents. Very nearly quantitative agreement with the experimental results is obtained.

The 15 cm^{-1} value of H_{ILET} is consistent with the nonadiabatic treatment of the acetonitrile data and the adiabatic treatment of the ethylene glycol data. Equation 3 yields adiabaticity parameters of 0.047 and 4.0 for acetonitrile and ethylene glycol, respectively. H_{ILET} is also small compared to room temperature thermal energies ($kT = 210$ cm^{-1}). Thus these calculations are consistent with the MLCT state being localized on a single ligand, which was a central premise of the above analysis. We conclude that with respect to adiabaticity and ligand localization the analysis is completely self-consistent. The 500 cm^{-1} value of $\Delta G^{\ddagger}$ may be used, along with the solvent dielectric parameters, to estimate a value of the MLCT dipole, using eq 7. A value of 9.9 D is obtained, which is close to the experimental value reported in ref 5.

Time-and x-dependent populations on the reactant and product potential surfaces are determined in the above model calculations. From the analysis of these populations, it is possible to assign which relaxation processes are responsible for the observed kinetic components in the depolarization decays shown in Figures 7 and 8. In the case of acetonitrile, the situation is trivially simple. Boltzmann distributions are maintained in both reactant and product wells, and the depolarization kinetics reflect the TST reaction rate and rotational diffusion. The situation is more complicated in slowly relaxing and hence adiabatic ethylene glycol. In this case, relaxation processes must be considered in terms of upper, lower, and product potential energy surfaces as depicted in Figure 6. Furthermore, it must be kept in mind that the upper surface is reactant-like ($x < 0$) or product-like ($x > 0$) away from the avoided crossing. The opposite is true of the lower surface. Several different types of relaxation processes can occur on these surfaces. Which processes are involved depends upon where the initial population starts out, i.e., the dynamics are excitation wavelength dependent. Consider the case of 664 nm excitation. This is blue of the absorption onset and puts population on the upper surface at x

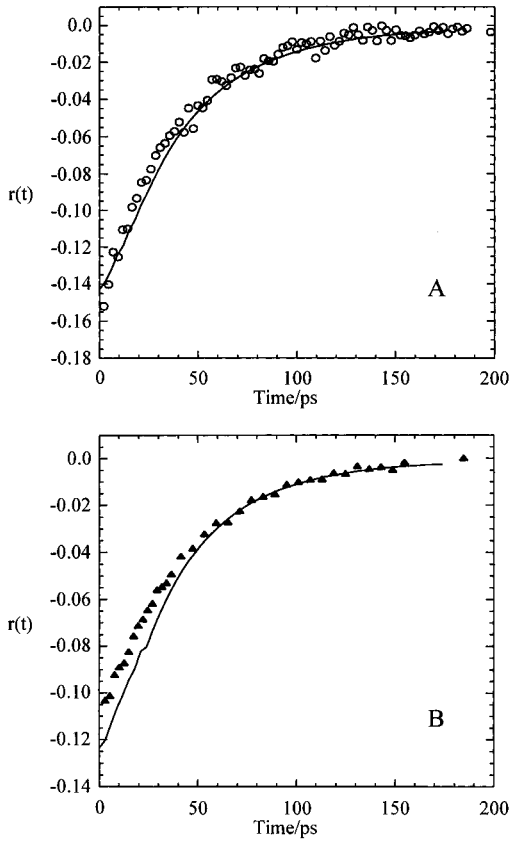

Figure 7. Plots comparing the calculated depolarization ratio for $Os^{II}(bpy)_3$ in room temperature acetonitrile (lines) with the experimental depolarization ratio (symbols). (A) The experimental data is the 664 nm pump, 332 nm probe. The A_1 and A_2 values in eq 20 are −0.45 and −0.1125, respectively, for the calculated curve. (B) The experimental data is the 690 nm pump, 345 nm probe. The A_1 and A_2 values in eq 20 are −0.375 and −0.0375, respectively, for the calculated curve. The calculated curves in both parts A and B have been convoluted with the measured instrument response function, as discussed in the text. In both cases, the calculated curves correspond to $\Delta G^{\ddagger} = 500$ $cm^{-1}$and $H_{ILET} = 15$ cm^{-1}.

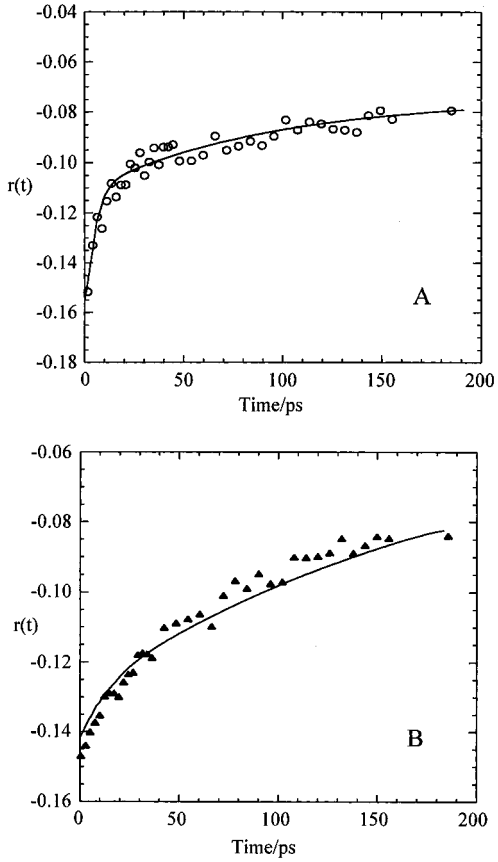

Figure 8. Plots comparing the calculated depolarization ratio for $Os^{II}(bpy)_3$ in room temperature ethylene glycol (lines) with the experimental depolarization ratio (symbols). (A) The experimental data is the 664 nm pump, 332 nm probe. The A_1 and A_2 values in eq 20 are −0.45 and −0.1125, respectively, for the calculated curve. (B) The experimental data is the 690 nm pump, 345 nm probe. The A_1 and A_2 values in eq 20 are −0.375 and are −0.0375, respectively, for the calculated curve. The calculated curves in both parts A and B have been convoluted with the measured instrument response function, as discussed in the text. In both cases, the calculated curves correspond to $\Delta G^{\ddagger} = 500$ $cm^{-1}$and $H_{ILET} = 15$ cm^{-1}.

< 0. This population first relaxes to the bottom of the upper well (at $x = 0$) at the solvent relaxation rate. At $x = 0$, the upper well has equal components of reactant and product character. This relaxation therefore corresponds to a significant reactant−product conversion, with the resulting change in absorption depolarization. Ethylene glycol has an average solvent relaxation time of 15 ps, and the corresponding fast depolarization kinetic component is seen in Figure 8A. It is of interest to note that the average ethylene glycol relaxation time determined by time-dependent Stokes shift measurements[32] is ∼15 ps, and this value results in a good fit with the present results. The bulk average longitudinal relaxation time of ethylene glycol is about 80 ps[40] which results in very poor agreement with these results. We conclude that in this case, solvent dynamics are adequately described only by the microscopically determined relaxation rates.

Following relaxation to the bottom of the upper well, the population may subsequently hop to the lower and product-like potential surfaces with a further change in the absorption depolarization. This occurs with a rate given by eq 13 and dominates the 30−200 ps kinetics shown in Figure 8A.

Photoexcitation at 690 nm results in a very different initial population distribution and thus very different dynamics. In this case, the population starts out at $x > 0$ on the reactant curve. This is below the $x = 0$ transition state. As a result, the upper surface is simply not involved in the dynamics. The vast majority of this population relaxes on the lower surface, and reactant−product conversion occurs by adiabatic crossing of the barrier. This process dominates the calculated curve shown in Figure 8B.

It is possible to comment on the qualitative aspects of the glycerol results shown in Figure 4 based upon these calculations. The glycerol results are qualitatively similar to those obtained in ethylene glycol. The blue excitation (664 and 682 nm) kinetics show a fast component which is absent in the 690 nm excitation kinetics. This component may be assigned to initial motion on the upper potential surface. The rapid time scale of this decay component indicates that, despite the overall slow relaxation rate, some solvent relaxation occurs rapidly. This is consistent with the strongly non-Debye nature of alcohol and polyalcohol solvents.

It is also possible to comment on our previous $Ru^{II}(bpy)_3$ ILET results in light of these calculations.[19] Because of the lack of variation of excitation wavelength and the limited temporal resolution of those experiments (∼45 ps) only qualitative or semiquantitative comparisons can be made. Despite the above caveats, it is possible to fit the $Ru^{II}(bpy)_3$ results in both ethylene glycol and acetonitrile using the same H_{ILET} (=15 cm^{-1}) and $\Delta G^{\ddagger}$ (=500 cm^{-1}) parameters as in the above $Os^{II}(bpy)_3$ case. We conclude that the same qualitative dynamics occur in both systems.

Conclusions

The ILET dynamics of $Os^{II}(bpy)_3$ in it's MLCT state have been elucidated using time-resolved absorption polarization spectroscopy. The results are shown to be strongly dependent upon the solvent relaxation dynamics, and, in the slowly relaxing solvents, upon the excitation wavelength. These results may be understood by comparison with model calculations. The conclusions resulting from this comparison may be summarized as follows.

(1) The ILET dynamics in acetonitrile are independent of the excitation wavelength and characterized by a single rate constant. Boltzmann distributions are maintained in reactant and product wells, and the rate constant is given by transition-state theory in the nonadiabatic limit.

(2) Ethylene glycol relaxes slowly, and the ILET dynamics are strongly excitation wavelength dependent in this solvent. Two major kinetic components are observed following (blue) excitation above the transition state: first, a very fast component that is assigned to relaxation to the bottom of the upper adiabatic surface; second, a slower component which is assigned to crossing to the lower adiabatic surface. A single, much slower kinetic component is observed following (red) excitation below the transition state. This component is assigned to adiabatic barrier crossing on the lower surface.

(3) Use of the average bulk longitudinal relaxation time results in a poor fit to the data presented here, while use of the (microscopic) relaxation time determined from dynamic Stokes shift measurements results in a very good fit.

Acknowledgment. This work was supported by a grant from the National Science Foundation.

References and Notes

(1) (a) Dallinger, R. F.; Woodruff, W. H. *J. Am. Chem. Soc.* **1979**, *101*, 4391. (b) Bradley, P. G.; Kressn, N.; Hornberger, B. A.; Dallinger, R. F.; Woodruff, W. H.; *J. Am. Chem. Soc.* **1981**, *103*, 7441.

(2) McClanahan, S. F.; Dallinger, R. F.; Holler, F. J.; Kincaid, J. R. *J. Am. Chem. Soc.* **1985**, *107*, 4853.

(3) Smothers, W. K.; Wrighton, M. A. *J. Am. Chem. Soc.* **1983**, *103*, 1051. Mabrouk, P. A.; Wrighton, M. A. *Inorg. Chem.* **1986**, *25*, 526.

(4) Carrol, P. J.; Brus, L. E. *J. Am. Chem. Soc.* **1987**, *109*, 7613.

(5) Kober, E. M.; Sulivan, B. P.; Meyer, T. J. *Inorg. Chem.* **1984**, *23*, 2098.

(6) Kato, M.; Yamauchi, S.; Hirota, N. *J. Phys. Chem.* **1989**, *93*, 3422.

(7) Striplin, D. R.; Crosby, G. A. *Chem. Phys. Lett.* **1994**, *221*, 426.

(8) Carlin, C. M.; DeArmond, M. K. *Chem. Phys. Lett.* **1982**, *89*, 297.

(9) Myrick, M. L.; Blakley, R. L.; DeArmond, M. K.; Arthur, M. L. *J. Am. Chem. Soc.* **1988**, *110*, 1325.

(10) Riesen, H.; Krausz, E. *Chem. Phys. Lett.* **1993**, *212*, 347.

(11) Riesen, H.; Gao, Y.; Krausz, E. *Chem. Phys. Lett.* **1994**, *228*, 610.

(12) Riesen, H.; Wallace, L.; Krausz, E. *J. Chem. Phys.* **1995**, *102*, 4823; *Mol. Phys*. **1996**, *87*, 1299.

(13) Riesen, H.; Rae, A. D.; Krausz, E. *J. Lumin.* **1994**, *62*, 123. Riesen, H.; Wallace, L.; Krausz, E. *Chem. Phys.* **1995**, *198*, 269.

(14) Riesen, H.; Wallace, L.; Krausz, E. *Chem. Phys. Lett.* **1994**, *228*, 605.

(15) Riesen, H.; Krausz, E. *Chem. Phys. Lett.* **1994**, *217* 613.

(16) Huber, P.; Yersin, H. *J. Phys. Chem.* **1993**, *97*, 12705.

(17) Chung, Y. C.; Leventis, N.; Wagner, P. J.; Leroi, G. E. *Inorg. Chem.* **1985**, *24*, 1965; *J. Am. Chem. Soc*. **1985**, *107*, 1416.

(18) Cooley, L. F.; Bergquist, P.; Kelley, D. F. *J. Am. Chem. Soc.* **1990**, *112*, 2612.

(19) Malone, R. A.; Kelley, D. F. *J. Chem. Phys.* **1991**, *95*, 8970.

(20) Pogge, J. L.; Kelley, D. F. *Chem. Phys. Lett.* **1995**, *238*, 16.

(21) Turr, C.; Chung, Y. C.; Leventis, N.; Kuchenmeister, M. E.; Wagner, P. J.; Leroi, G. E. *Inorg. Chem.* **1996**, *35*, 5104.

(22) Hupp, J. T. Private communication; *Inorg. Chem.*, submitted.

(23) Orman, L. K.; Change, Y. J.; Anderson, D. R.; Yabe, T.; Xu, X.; Yu, S−C.; Hopkins, J. B. *J. Chem. Phys.* **1989**, *90*, 1469.

(24) (a) Cooley, L. F.; Headford, C. E. L.; Elliott , C. M.; Kelley, D. F. *J. Am. Chem. Soc.* **1988**, *110*, 6673. (b) Cooley, L. F.; Larson, S. L.; Elliott, C. M.; Kelley, D. F. *J. Phys. Chem.* **1991**, *95*, 10694.

(25) Creutz, C.; Chow, M.; Netzel, T.; Okumura, M.; Sutin, N. *J. Am. Chem. Soc*. **1980**, *102*, 1309.

(26) Konig, E.; Kremer, S. *Chem. Phys. Lett.* **1970**, *5*, 87.

(27) Carlin, C. M.; DeArmond, M. K. *J. Am. Chem. Soc.* **1985**, *107*, 53.

(28) Albrecht, A. *J. Mol. Spectrosc.* **1961**, *6*, 84.

(29) Fleming, G. R. *Chemical Applications of Ultrafast Spectroscopy*; Oxford University Press: New York, 1986.

(30) Frauenfelder, H.; Wolynes, P. *Science* **1985**, *229*, 337.

(31) (a) Landau, L. *Sov. Phys.* **1932**, *1*, 89. (b) Landau, L. *Z. Phys. Sov.* **1932**, *2*, 1932. (c) Zener, C. *Proc. R. Soc. Ser. A.* **1932**, *137*, 696. (d) Stueckelberg, E. *Helv. Phys. Acta* **1932**, *5*, 369. (e) Eryring, H.; Walter, J.; Kimball, G. *Quantum Chemistry*; Wiley: New York, 1944.

(32) Maroncelli, M.; *J. Mol. Liquids* **1993**, *57*, 1.

(33) (a) Barbara, P.; Jarzeba, W. *Adv. in Photochem.* **1990**, *15*, 1. (b) van der Zwan, G.; Hynes, J. *J. Phys. Chem.* **1985**, *89*, 4181.

(34) Jortner, J.; Bixon, M. *J. Chem. Phys.* **1988**, *88*, 167.

(35) Pauling, L.; Wilson, E. *Introduction to Quantum Mechanics*; Dover Publications, Inc.: New York, 1963.

(36) (a) von Smoluchowski, M. *Ann. Phys.* **1915**, *48*, 1103. (b) von Smoluchowski, M. *Z. Phys. Chem.* **1917**, *92*, 129. (c) Wilemski, G. *J. Stat. Phys.* **1976**, *14*, 153.

(37) Agmon, N.; Hopfield, J. *J. Chem. Phys.* **1983**, *78*, 6947.

(38) Hynes, J. *J. Phys. Chem.* **1986**, *90*, 3701.

(39) Tao, T. *Biopolymers* **1969**, *8*, 609.

(40) Simon, J. D. *Acc. Chem. Res.* **1988**, *21*, 128.